THE JOURNAL OF BIOLOGICAL CHEMISTRY VOL. 286, NO. 33, pp. 29175–29191, August 19, 2011

Building Blocks of the Nexin-Dynein Regulatory Complex in *Chlamydomonas* Flagella*[S]

Received for publication, March 21, 2011, and in revised form, June 13, 2011 Published, JBC Papers in Press, June 23, 2011, DOI 10.1074/jbc.M111.241760

Jianfeng Lin[‡], Douglas Tritschler[§], Kangkang Song[‡], Cynthia F. Barber[‡], Jennifer S. Cobb[¶], Mary E. Porter[§], and Daniela Nicastro[‡1]

From the [‡]Biology Department, Rosenstiel Center, MS029, Brandeis University, Waltham, Massachusetts 02454, the [§]Department of Genetics, Cell Biology, and Development, University of Minnesota, Minneapolis, Minnesota 55455, and the [¶]Chemistry Department, MS015, Brandeis University, Waltham, Massachusetts 02454

The directional flow generated by motile cilia and flagella is critical for many processes, including human development and organ function. Normal beating requires the control and coordination of thousands of dynein motors, and the nexin-dynein regulatory complex (N-DRC) has been identified as an important regulatory node for orchestrating dynein activity. The nexin link appears to be critical for the transformation of dynein-driven, linear microtubule sliding to flagellar bending, yet the molecular composition and mechanism of the N-DRC remain largely unknown. Here, we used proteomics with special attention to protein phosphorylation to analyze the composition of the N-DRC and to determine which subunits may be important for signal transduction. Two-dimensional electrophoresis and MALDI-TOF mass spectrometry of WT and mutant flagellar axonemes from *Chlamydomonas* identified 12 N-DRC-associated proteins, including all seven previously observed N-DRC components. Sequence and PCR analyses identified the mutation responsible for the phenotype of the *sup-pf-4* strain, and biochemical comparison with a radial spoke mutant revealed two components that may link the N-DRC and the radial spokes. Phosphoproteomics revealed eight proteins with phosphorylated isoforms for which the isoform patterns changed with the genotype as well as two components that may play pivotal roles in N-DRC function through their phosphorylation status. These data were assembled into a model of the N-DRC that explains aspects of its regulatory function.

Cilia and flagella are important motility and sensory organelles in eukaryotes. These organelles are ubiquitous and conserved from single-celled protists, such as the green algae *Chlamydomonas,* to humans, where motile and nonmotile cilia are involved in proper embryonic development and organ function. Dysfunction of cilia or flagella is associated with several human diseases, such as polycystic kidney disease, polycystic liver disease, primary ciliary dyskinesia, Bardet-Biedl syndrome, Meckel-Gruber syndrome, Joubert syndrome, hydrocephalus, and infertility (1, 2). Motile flagella are also essential for successful host infection by pathogenic flagellates, such as *Trypanosoma brucei*, which causes sleeping sickness (3, 4), making these organelles potential drug targets.

The core structure of most motile cilia and flagella is the 9+2 axoneme, which consists of the central pair complex and nine surrounding doublet microtubules (DMTs).[2] This assembly associates with motor enzymes, radial spokes, and the nexin-dynein regulatory complex (N-DRC), which connects each DMT with its two neighbors (Fig. 1*A*) (5–7). The force-producing dynein motors are attached in two rows, the inner and outer dynein arms, along the length of the A-tubule of each DMT (Fig. 1, *B* and *C*). The dyneins walk along the B-tubule of the neighboring DMT to generate sliding forces between the doublets. Restriction of this sliding motion, *e.g.* by the N-DRC, is thought to convert sliding forces into bending of the axoneme (8, 9). Formation of bending in different directions and traveling waves require the precise coordination of the activity of the tens of thousands of dyneins in a single axoneme. Genetic, structural, and biochemical studies of *Chlamydomonas* flagella suggest that several axonemal complexes are involved in this regulation. The central pair complex and radial spokes (CPC·RS) (10), the I1 inner dynein arm present on the proximal end of the 96-nm repeat (5, 11, 12), and the N-DRC on the distal end of the repeat (7, 13) are all thought to transmit mechanical and/or chemical signals that control dynein function and thus ciliary and flagellar beating.

Our recent ultrastructural study has not only revealed that the nexin link, a classically defined connection between adjacent DMTs, is an integral part of the dynein regulatory complex (which is therefore now called the "nexin-dynein regulatory complex") but also revealed that the N-DRC is a highly connected regulatory hub within the axoneme (7). The identification of the nexin link opens the way to understand how the relative position of DMTs, which changes during wave propagation, can control dynein function. However, the exact nature of this control is still unknown. Like the I1 dynein, the N-DRC appears to be ideally situated to mediate signaling from the CPC·RS complex to the dynein arms (7, 14). Furthermore,

* This work was supported, in whole or in part, by National Institutes of Health Grants GM083122 (to D. N.) and GM55667 (to M. E. P.). This work was also supported by a Pew Scholars award (to D. N.).

[S] The on-line version of this article (available at http://www.jbc.org) contains supplemental Figs. S1–S4 and Table S1.

[1] To whom correspondence should be addressed: MS029, Brandeis University, 415 South St., Waltham, MA 02454-9110. Tel.: 781-736-2408; Fax: 781-736-2419; E-mail: nicastro@brandeis.edu.

[2] The abbreviations used are: DMT, doublet microtubule; N-DRC, nexin-dynein regulatory complex; CPC, central pair complex; RS, radial spoke; cryo-ET, cryo-electron tomography; 2DE, two-dimensional electrophoresis; FAPs, flagellar associated proteins; PMF, peptide mass fingerprinting; PTM, post-translational modification; qRT, quantitative RT; LRR, leucine-rich repeat; CSC, CaM- and radial spoke-associated complex.

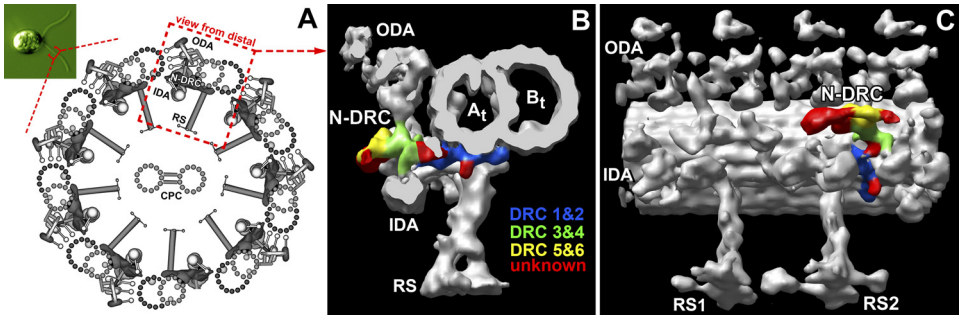

FIGURE 1. **Models showing the N-DRC in *Chlamydomonas* flagella.** *A,* differential interference contrast image showing a *Chlamydomonas* cell with its two flagella and a zoomed in schematic of a flagellar axoneme in cross-sectional view, seen from the flagellar tip. Three structures that connect neighboring doublets are as follows: IDAs, ODAs, and the N-DRC complex. *B* and *C,* three-dimensional maps of the 96-nm axonemal repeat in WT *Chlamydomonas* flagella reconstructed by cryo-electron tomography (cryo-ET), in cross-sectional (*B*) and longitudinal views (*C*). The suggested locations of N-DRC subunits are summarized and colored. A_t, A-tubule; B_t, B-tubule; *CPC,* central pair complex; *IDA,* inner dynein arm; *ODA,* outer dynein arm; *RS,* radial spoke. Images are adapted from Heuser *et al.* (7).

TABLE 1
Strains used in this study and summary of previous biochemical studies

Name	Strain	Phenotype[a]	Previously observed N-DRC components[b]						
			1	2	3	4	5	6	7
WT	CC-125, 137c mt+	WT waveform, fast swimming	+	+	+	+	+	+	+
PF2-HA[c]	*pf2–4::PF2-HA*	WT waveform, fast swimming	+	+	+	+	+	+	+
pf3	CC-1026, *pf3*	Abnormal waveform, slow swimming	−	−	+	+	−	−	+
sup-pf-4	CC-2366, *sup-pf-4*	WT waveform, slightly slower swimming	+	+	+	+	−	−	+
sup-pf-3	CC-1399, *sup-pf-3*	Abnormal waveform, slow swimming	+	+	+/−	−	+/−	+/−	+
pf2[c]	*pf2-4*	Abnormal waveform, slow swimming	+	+	−	−	−	−	−
pf9-3[d]	CC-3913	Slow swimming	Not determined						
pf14	CC1032, mt+	Paralyzed	Not determined						

[a] Phenotype information is from Brokaw and Luck (27), Brokaw and Kamiya (28), Gardner *et al.* (14), and Rupp and Porter (13).
[b] + indicates component present; +/− indicates component reduced; − indicates component absent. Abundance information is from Huang *et al.* (15), Piperno *et al.* (16), Piperno *et al.* (17), and Rupp and Porter (13).
[c] Data are from Rupp and Porter (13).
[d] Data are from Myster *et al.* (65).

mutations that alter the assembly of the N-DRC subunits partially suppress paralysis caused by defects in the CPC·RS (15–17); this finding suggests that the N-DRC acts as an inhibitor of dynein activity in the absence of signals from the CPC·RS complex. Several studies have also indicated that the CPC·RS regulates dynein activity through the phosphorylation of I1 dynein (12, 18–20). Given that several kinases and phosphatases, such as CK1, PP1, and PP2A, are anchored in the axoneme (20–24), and several axonemal phosphoproteins have been detected (25, 26), it is possible that the regulatory mechanism used by the N-DRC also involves a phosphorylation pathway. However, little is known about the composition, post-translational modification (PTM) profile, or regulatory mechanism of the N-DRC.

Chlamydomonas reinhardtii is a well established model organism with a large arsenal of available mutants, including *drc* mutants (15–17, 27, 28), which have recently been shown to have specific structural defects in the N-DRC and some associated structures, such as the inner dynein arms that attach directly to the N-DRC (7, 13, 14, 29). Biochemical and structural studies have shown additional defects in these mutants, such as reduced levels of tektin and radial spoke components; however, the relationship between these defects and the N-DRC is not well understood (14, 16, 17, 30). Early proteomics studies employed SDS-PAGE and two-dimensional electrophoresis (2DE) to compare the axonemal proteomes of WT and *drc* mutants, revealing seven polypeptides that changed in abundance significantly in the mutants (15–17). These polypeptides were named DRC1–7 according to their molecular weights and order of discovery. Subsequent work has revealed that the *PF2* gene product, DRC4, is the *Chlamydomonas* ortholog of GAS8/GAS11/trypanin and that mutations in trypanin/GAS8 cause severe defects in *Trypanosoma* and zebrafish (4, 31). The identity of the remaining gene products has remained unknown.

Based on a comparison of the structure of *drc* mutant axonemes with that of WT *Chlamydomonas* axonemes, we recently proposed a model for the locations of DRC1–7 within the N-DRC (7). The results suggested that there are additional unknown N-DRC components (7). In a 2005 proteomics study of *Chlamydomonas* flagella, more than 600 flagellar proteins were identified by MS (24). Most of these proteins had not been previously characterized and were simply named "flagellar associated proteins" (FAPs). Many of the N-DRC components are likely to be among these flagellar associated proteins. Technological advances in proteomics and the identification of PTMs, as well as the sequencing of the *C. reinhardtii* genome, now make it possible to identify both previously reported and novel genes encoding the N-DRC components and to shed light on their functions. Therefore, we used gel-based proteomic approaches to identify the components of the N-DRC in the *C. reinhardtii* axoneme, to determine their defects in *drc* mutants, and to characterize their phosphorylation states. Twelve N-DRC candidates, including DRC1–7, were identified and characterized in this study. Two components are likely involved in the connection between the N-DRC and the RS, and the phosphorylation of at least two subunits has been shown to be

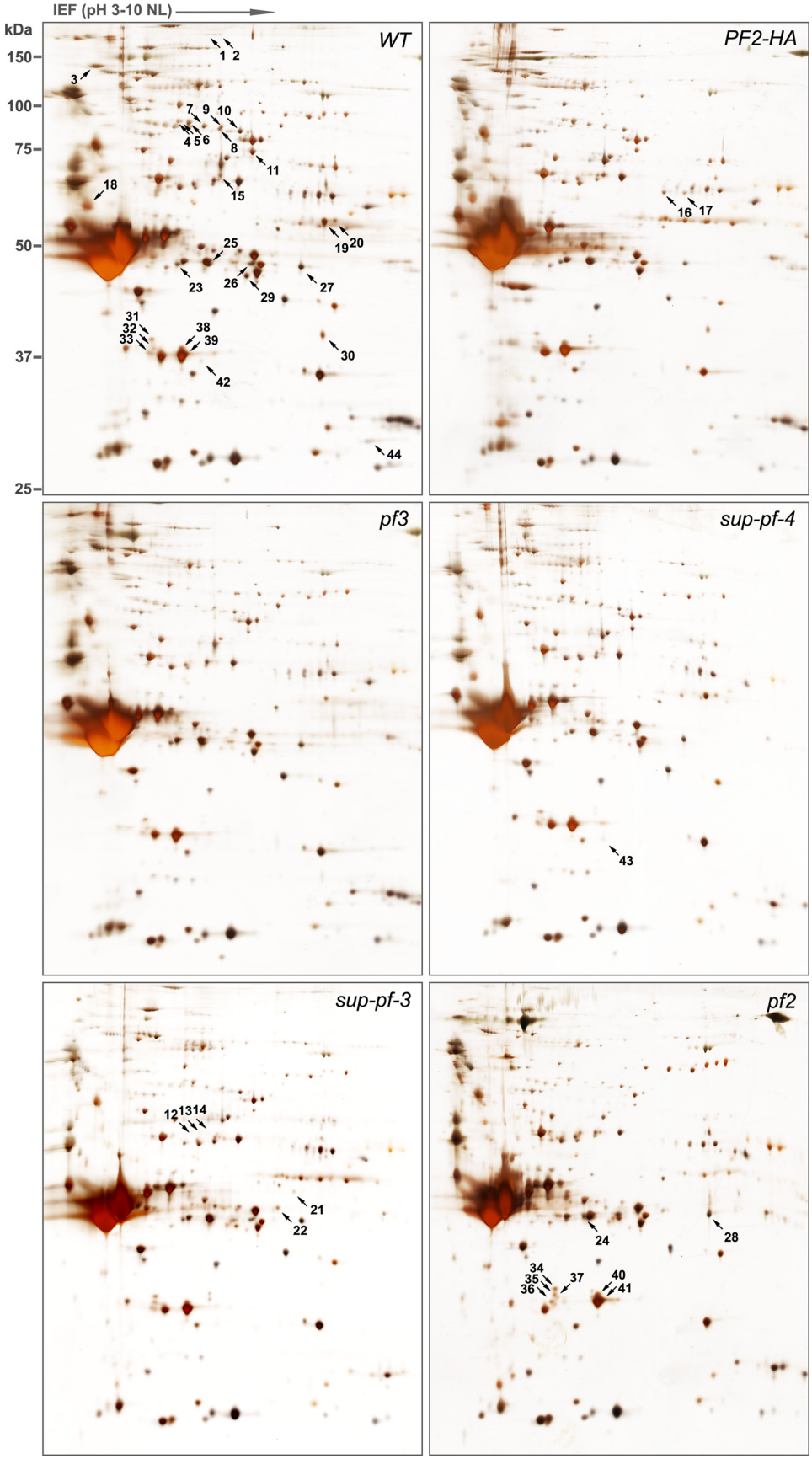

FIGURE 2. **Comparison of the axonemal polypeptides from WT *Chlamydomonas*, a rescued *pf2* strain (*PF2-HA*) and four *drc* mutants (*pf3*, *sup-pf-4*, *sup-pf-3*, and *pf2*) using 2DE (with silver staining).** *Arrows,* polypeptides with significantly altered abundance.

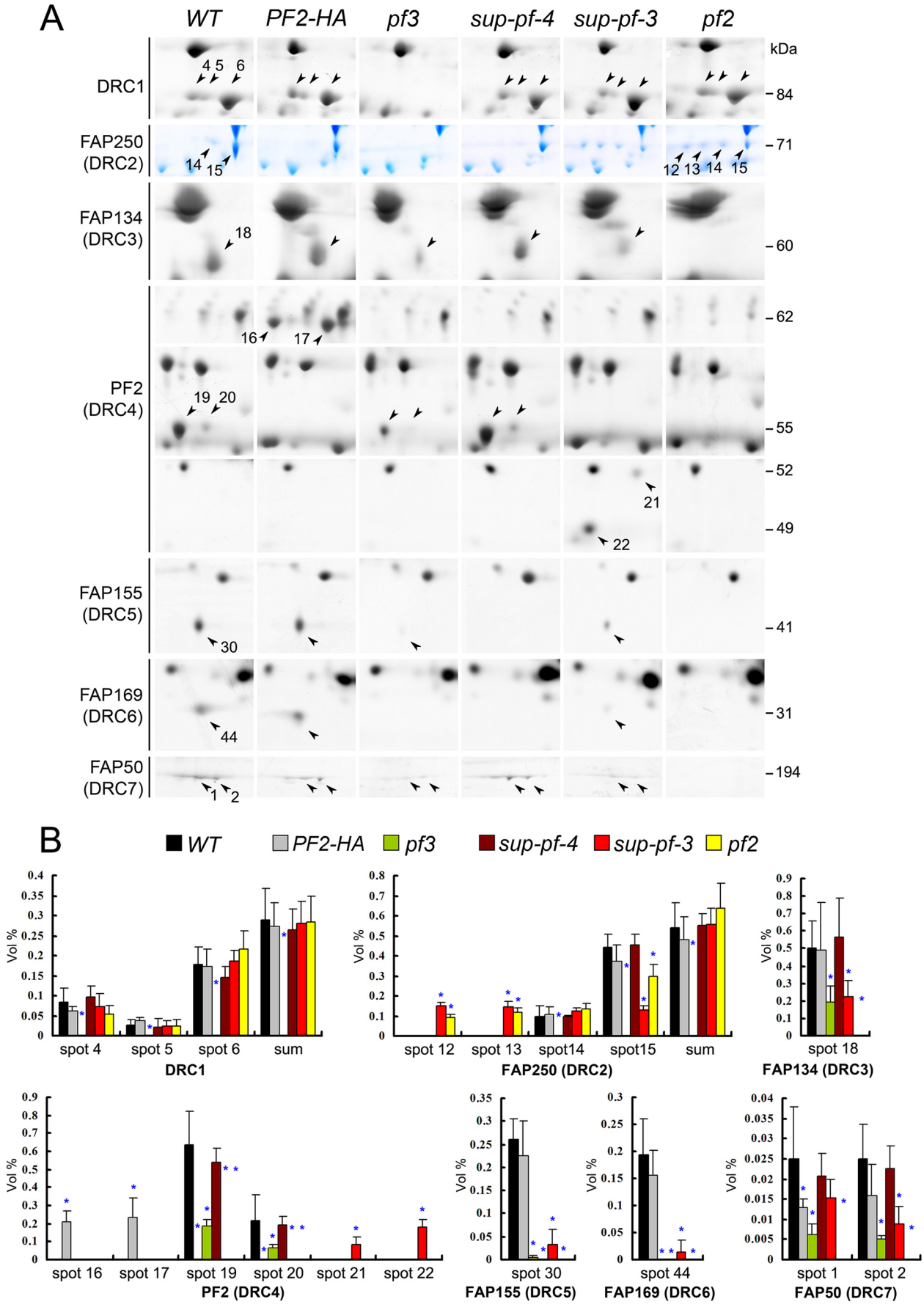
A
WT
PF2-HA
pf3
sup-pf-4
sup-pf-3
pf2
kDa
DRC1
FAP250 (DRC2)
FAP134 (DRC3)
PF2 (DRC4)
FAP155 (DRC5)
FAP169 (DRC6)
FAP50 (DRC7)
84
71
60
62
55
52
49
41
31
194
B
WT
PF2-HA
pf3
sup-pf-4
sup-pf-3
pf2
Vol %
spot 4
spot 5
spot 6
sum
DRC1
spot 12
spot 13
spot14
spot15
sum
FAP250 (DRC2)
spot 18
FAP134 (DRC3)
spot 16
spot 17
spot 19
spot 20
spot 21
spot 22
PF2 (DRC4)
spot 30
FAP155 (DRC5)
spot 44
FAP169 (DRC6)
spot 1
spot 2
FAP50 (DRC7)

important for the activity of flagella. These results provide N-DRC components that could potentially be critical for the regulation of dynein activity, give insights into the process of N-DRC assembly, lay the foundation for future studies into the role of the N-DRC in regulating flagellar beating, and could ultimately lead to better understanding and treatment of ciliopathies in humans.

EXPERIMENTAL PROCEDURES

Strains and Culture Conditions—*C. reinhardtii* strains used in this study are listed in Table 1. Cells were grown in liquid Tris acetate/phosphate medium (32), primarily with a light/dark cycle of 16:8 h but under continuous light conditions for qRT-PCR analysis.

Axonemal Sample Preparation—Axonemes were isolated using the pH shock method as described previously (33, 34). For the N-DRC proteome study, axonemes were prepared directly in 2DE lysis buffer (7 M urea, 2 M thiourea, 4% CHAPS, 65 mM DTT, and 2% IPG buffer (pH 3–10NL; GE Healthcare)). For phosphorylation analysis, the proteins were treated with λ-protein phosphatase as described previously (36, 37).

Gel Electrophoresis—Protein gel electrophoresis was performed as described previously, with slight modifications (37). Briefly, for SDS-PAGE analysis, 15 μg of axonemal protein (or 30 μg for preparative gels) was separated on a 5% SDS-polyacrylamide gel (260 × 200 × 1 mm). For 2DE analysis, 70 μg of axonemal protein (300 μg for preparative gels) was separated on 13-cm immobilized pH 3–10 nonlinear gradient dry strips (GE Healthcare) for a total of 24 kV-h (34 kV-h for preparative gels) and then separated on a 10% SDS-polyacrylamide gel (260 × 200 × 1 mm). All axonemal samples (3–7 samples for each strain) were run at least in duplicate to guarantee reproducibility.

Staining and Image Acquisition—Silver nitrate and colloidal Coomassie Blue were used to stain polypeptides resolved on analytical gels and preparative gels, respectively. In addition, Pro-Q Diamond (Invitrogen) was used to probe for phosphorylation, according to the manufacturer's instructions. Pro-Q Diamond signals were visualized with a Typhoon 9410 variable mode imager (GE Healthcare) using a 532-nm laser for excitation and a 560-nm long pass filter for emission. Following image acquisition, gels were post-stained with SYPRO Ruby (Invitrogen) to detect total protein.

Statistical Analysis—2DE images were analyzed using ImageMaster™ 2D Platinum software (Version 5.0; GE Healthcare). Protein spots were detected automatically and then manually edited. Large tubulin spots were oversaturated on silver-stained gels and were therefore excluded from the analysis. Individual spot volumes were normalized against total spot volumes to compensate for nonabundance-related variations in spot quantities between gels. Two-sample *t* tests were used to analyze differences in protein abundance between WT and mutant samples. Values of p less than 0.05 were considered statistically significant. Spots changing significantly in abundance (over ±1.5-fold) in the *drc* mutants compared with the WT cells were taken as N-DRC candidate components.

Tryptic In-gel Digestion and MALDI-TOF MS—Spots of interest were excised from the preparative gels and digested with trypsin as described previously (37). Mass spectra were obtained using a Bruker Daltonics Microflex mass spectrometer. Peptide mass fingerprinting (PMF) was interpreted by the Mascot sequence database search engine configured with a mass tolerance of 50 ppm and the variable modifications "carbamidomethylation of cysteine and oxidation of methionine" using the NCBI database. Probability-based MASCOT scores were used to evaluate identifications. Peptide mixtures that yielded statistically significant search scores (>95% confidence interval, equivalent to an expected MASCOT value <0.05) and accounted for the majority of ions present in the mass spectra were defined as positive identifications.

qRT-PCR, Genomic PCR, and DNA Sequencing— qRT-PCR analysis was performed as described previously using the $2^{-\Delta\Delta Ct}$ method (38–40). *CβLP* (41) was used as the endogenous control for calculation of relative abundances. Relative transcript abundances for the mutants were standardized to WT. To confirm the gene defect in *sup-pf-4*, genomic DNA was isolated from WT, *sup-pf-4*, and *pf25* (the parent strain for *sup-pf-4*). Eight PCR primers were designed to amplify genomic DNA fragments in the region around *FAP155* (Fig. 7*C*). Four PCR primers spanning the *FAP169* transcription unit were designed to amplify selected fragments for DNA sequencing (supplemental Fig. S3). The resulting PCR products were separated by agarose gel electrophoresis.

Bioinformatic Analysis—A stringent reciprocal BLASTP (42) protocol was used to identify homologs of the identified *Chlamydomonas* proteins. The on-line BLAST server at NCBI (www.ncbi.nlm.nih.gov) was used to search all predicted proteins of the query organisms *Volvox carteri* (taxid:3067), *Strongylocentrotus purpuratus* (taxid:7668), *Homo sapiens* (taxid:9606), *Trypanosoma brucei* (taxid: 5691), *Arabidopsis thaliana* (taxid:3702), and *Caenorhabditis elegans* (taxid:6239), with an entry *e*-value cutoff of $1e^{-15}$ and all other standard settings. Domains and structural motifs within proteins were predicted using the on-line programs InterProScan, PFAM (INRA), SMART (EMBL, Heidelberg, Germany), MOTIF (GenomeNet), Multicoil (MIT), and COILS, using default parameters.

RESULTS

Comparative Proteomic Analysis of drc Mutants Identifies Known and Possibly Novel N-DRC Components—The proteins in axonemes isolated from WT *Chlamydomonas* and several *drc* mutants (Table 1) were separated on SDS-PAGE and 2DE gels and analyzed for statistically significant differences in pro-

FIGURE 3. **Details from 2DE analysis of WT, *PF2-HA,* and four *drc* mutants (*pf3*, *sup-pf-4*, *sup-pf-3,* and *pf2*) for the previously reported N-DRC components DRC1–7.** *A,* close-up images of 2DE gel spots of the proteins of interest. The images for DRC2 (FAP250) are from Coomassie-stained gels (*blue*), and all other images are from silver-stained gels. *Arrowheads,* spots showing significant differences in abundance between WT and *drc* mutants. *B,* relative protein quantification of spots with abundance differences between axonemes from WT and *drc* mutants. Relative quantifications are based on the average of 6–16 independently replicated silver-stained gels (or 2–4 Coomassie-stained gels for DRC2) and are expressed as the mean ± S.D. *Asterisks* indicate significant changes in comparison with WT (over ±1.5-fold; $p < 0.05$). *Spot numbers* correspond to the numbers depicted in Fig. 2 and Tables 2 and 3.

tein levels relative to WT. Protein spots that changed in abundance were selected for identification by MALDI-TOF MS. To obtain statistically significant results from the 2DE gels, axonemal proteins from the six cell lines were resolved on a total of 78 gels, of which 60 (6–14 per cell line) were stained with silver nitrate for image analysis (Fig. 2) and 18 (2–4 per cell line) were stained with colloidal Coomassie Blue for MS (supplemental Fig. S1). In total, 44 spots showed significant changes in protein level (over ±1.5-fold, $p < 0.05$) in the *drc* mutants compared with WT (Figs. 3 and 4). A comparison with published 2DE gels (15–17) indicates that these 44 spots include all of the previously described N-DRC components except for DRC7, which was only detected by SDS-PAGE in a previous study (17). To identify DRC7, axonemal proteins were also analyzed by 5% SDS-PAGE (Fig. 5). Each of the 44 spots with significant changes visible in 2DE gels (Fig. 2 and supplemental Fig. S1) and the DRC7 band separated in SDS-polyacrylamide gels were excised from at least two sets of Coomassie-stained gels for MALDI-TOF MS followed by PMF. NCBI database searches successfully identified the majority of the spots as 13 proteins (Tables 2 and 3). Two proteins, DRC1 and spot 11, could not be identified by PMF despite the presence of well resolved MS data (supplemental Fig. S2), suggesting that the corresponding genes are in regions of the *Chlamydomonas* genome that have not yet been sequenced or annotated.

The identified proteins fell into three categories as follows: (*a*) polypeptides with sizes, approximate spot positions, and the absence or presence in specific *drc* mutants corresponding to the previously described N-DRC components (15–17); (*b*) additional polypeptides that varied in abundance in different *drc* mutants, and (*c*) polypeptides with constant protein levels but with isoelectric points (pI) that were shifted in the first dimension in a given *drc* mutant. Each category is described in detail below.

Previous biochemical studies have reported unique abundance patterns for the first category of proteins, DRC1–7, in each of the *drc* mutants (Table 1) (15–17). However, the improved sensitivity of current proteomic techniques allowed us to determine the relative abundance of these proteins in WT and mutants with greater accuracy (Fig. 3 and Table 2). Refined abundance patterns provided additional details for DRC2–4 and -7. Another significant change from previous studies is the detection of multiple isoforms for most of the N-DRC proteins in our 2DE gels (Figs. 2 and 3; Table 2), although previously, the DRC components DRC1–7 have only been detected as single spots.

The sizes and locations of spots 4–6, and their absence in *pf3*, suggest that they represent the previously named DRC1 subunit (Figs. 2 and 3) (15–17). MS analysis of spot 6 produced high quality spectra with high similarity to the mass spectra of spots 4 and 5, indicating that all three spots are isoforms of the same protein (supplemental Fig. S2). However, the spectra could not be matched to a protein sequence in the NCBI database. Given the high quality of the spectra, the inability to identify a corresponding protein suggests that the sequence of DRC1 has not been entered in the database.

Spots 12–15 were not clearly detectable in the silver-stained gels but could be identified in the Coomassie-stained gels (Fig. 3 and supplemental Fig. S1). MS analysis identified the DRC2 spots as FAP250 (Table 2). Spots 12–14 represent isoforms of spot 15 found in a more acidic range of the gel; such isoforms had not previously been detected. Like DRC1, all DRC2 spots were absent from the *pf3* mutant. Spots 12 and 13 appeared only in the *sup-pf-3* and the *pf2* mutants; correspondingly, spot 15 was reduced in these two mutants (Fig. 3). These observations are also consistent with previous work from one of our laboratories identifying FAP250 as DRC2[3] and with recent work identifying CMF70, the trypanosome FAP250 homolog, as an N-DRC subunit (43).

The spot associated with DRC3 (spot 18) was identified as FAP134. 2DE gels confirmed previous data that DRC3 is missing in *pf2* and reduced in *sup-pf-3* (15–17). In addition, we observed a reduction in DRC3 abundance in *pf3* (Figs. 2 and 3). The reduction or lack of the spots associated with DRC5 and DRC6 (spots 30 and 44) also confirmed previous results (Figs. 2 and 3) (15–17). Here, we identified them as FAP155 and FAP169, respectively.

The previously identified component PF2 (DRC4) exhibited one of the most diverse abundance patterns among the strains, with a total of six different isoforms (Figs. 2 and 3). Two isoforms (spots 19 and 20) with similar molecular weights but different isoelectric points were present in WT, *sup-pf-4*, and *pf3*, although these spots were significantly reduced in *pf3* (Fig. 3). A different pair of isoforms with smaller molecular weights was present in *sup-pf-3*, and a final pair with higher molecular weights was present in the *PF2-HA* rescue strain (Fig. 3). These observations are consistent with previous studies showing that DRC4 is altered in *sup-pf-3* (15)[4] and restored to WT levels in the *PF2-HA* rescued strain (13).[5]

DRC7 was described previously as a band that was missing in SDS-polyacrylamide gels of *pf2* mutant axonemes (Table 1) (16). Here, we have correlated the DRC7 band with a series of spots on 2DE gels (Figs. 3 and 5). MS analysis identified the DRC7 band from SDS-polyacrylamide gels and two spots (spots 1 and 2) from the 2DE gels as FAP50. Consistent with previous studies, both SDS-PAGE and 2DE gels indicated that DRC7 is missing in *pf2* axonemes (Fig. 5). We also found that DRC7 is reduced in *sup-pf-3* and *pf3* axonemes (Figs. 3 and 5).

The second category of components, novel N-DRC candidates with differences in abundance in mutant strains, includes four proteins as follows: FAP61/IDA7, ICL1, and the unidentified spot 11 (Fig. 4 and Table 3). Spot 3, which was identified through MS as a mixture of two proteins, FAP61 and IDA7 (also called IC140), was a single blurry spot by 2DE and was reduced in all mutants (Fig. 4). Spot 11, which was reduced in *pf2*, *pf3*, and *sup-pf-3*, could not be matched to any known sequence in the NCBI database. The final spot (spot 29) was identified as ICL1; ICL1 levels were reduced in all mutants, but ICL1 was the only protein not restored in the *PF2-HA* rescued strain (Fig. 4 and Table 3).

The third category, novel N-DRC candidates with shifted pI values, includes four proteins as follows: FAP252, FAP230,

[3] D. Tritschler, R. Bower, and M. E. Porter, unpublished data.
[4] R. Bower, D. Tritschler, and M. E. Porter, unpublished data.
[5] R. Bower and M. E. Porter, unpublished data.

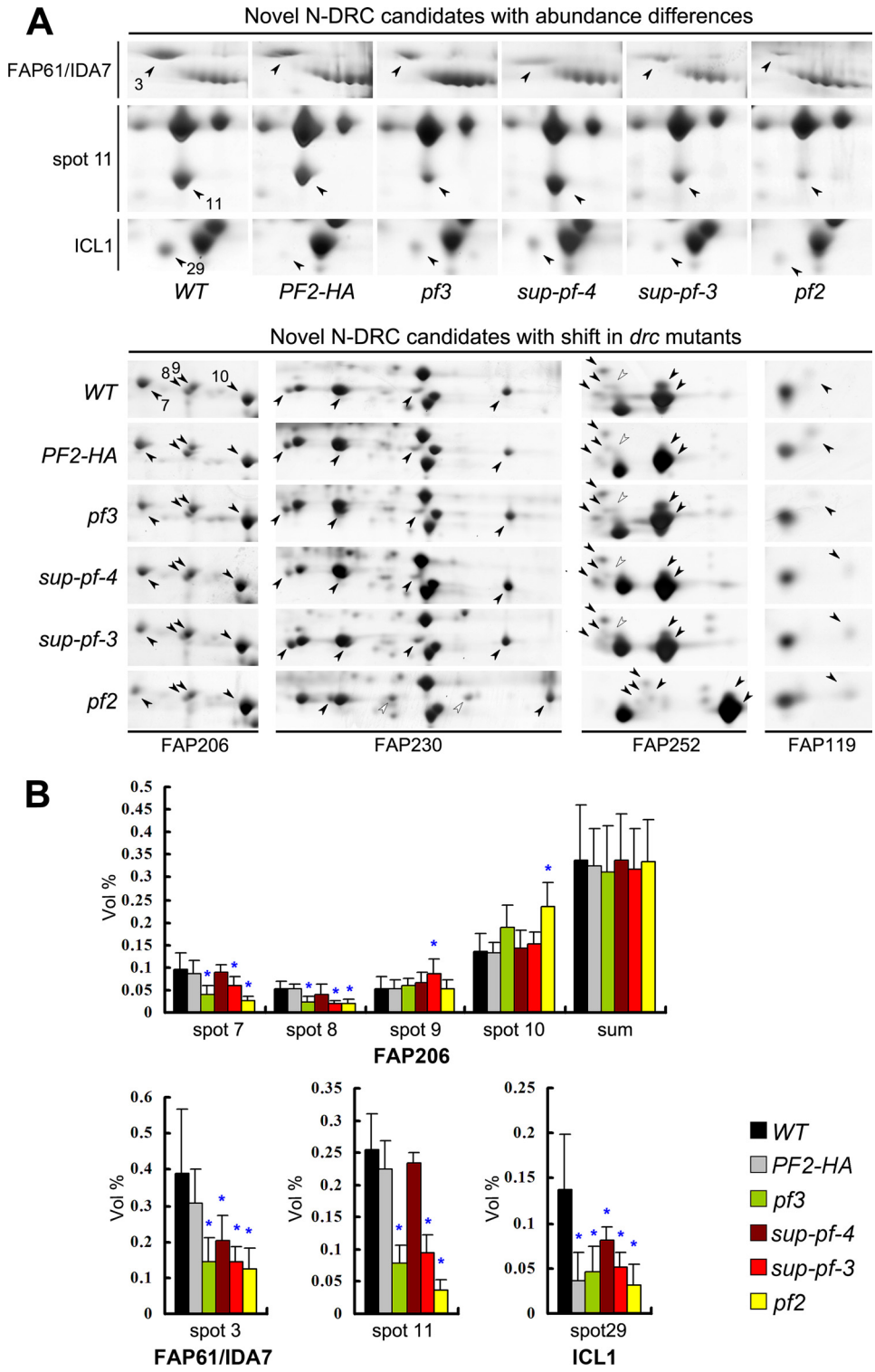

FIGURE 4. **Details from 2DE analysis of WT, *PF2-HA*, and four *drc* mutants (*pf3*, *sup-pf-4*, *sup-pf-3*, and *pf2*) for novel proteins that showed significant changes in abundance in the mutants.** *A*, close-up images of silver-stained 2DE gel spots of the proteins of interest. *Filled arrowheads* indicate spots with significant differences between WT and *drc* mutants. *Open arrowheads* indicate spots in the panels for FAP230 and FAP252 that were not analyzed by MS but that most likely correspond to one of the shifted spots in the *pf2* gels, based on the gel pattern. *B*, relative protein quantification of spots with abundance differences between axonemes from WT and *drc* mutants. Relative quantifications are based on the average of 6–16 independently replicated silver-stained gels and are expressed as the mean ± S.D. *Asterisks* indicate significant changes in comparison with WT (over ±1.5-fold; $p < 0.05$). *Spot numbers* correspond to the numbers depicted in Fig. 2 and Tables 2 and 3.

FAP119, and FAP206. Each of these proteins shifted toward the basic side in the first dimension in the *pf2* mutant. FAP119 also shifted to a more basic pI in *sup-pf-3* and *sup-pf-4*, whereas FAP206 shifted to a more basic pI in *sup-pf-3* and *pf3* (Fig. 4). FAP206 appeared as four spots, and all the mutants except for *sup-pf-4* showed differences in some of these four FAP206 iso-

forms; however, we found little change in the total amount of FAP206 protein in each cell line (Fig. 4). FAP252 appeared in at least 11 different spots on the 2DE gels, depending on the mutant. Six isoforms were present in all cell lines except for *pf2*, in which all of these isoforms were modified in a way that promoted their shift to a more basic pI (Figs. 2 and 4). Similar results were observed with FAP230; its four spots (spots 23, 25–27) were present in all strains except for *pf2*, appearing to be shifted to more basic positions in *pf2*.

The reintroduction of the WT *PF2* gene has previously been shown to rescue the motility defects of the *pf2* mutant, as well as the structural defects visible by EM (7, 13).[5] Our 2DE gels of the *PF2-HA* rescued strain confirmed biochemically that PF2 (DRC4) is assembled at WT levels, as well as all but one of the proteins identified here as N-DRC components (Figs. 2–5 and supplemental Fig. S1). ICL1, which is a metabolic enzyme (EC 4.1.3.1) that catalyzes the first step in the glyoxylate bypass in bacteria, fungi, and plants, was the only polypeptide not rescued. The abundance of mRNA encoding ICL1 appears to be increased during flagellar regeneration (44); however, it is controversial whether ICL1 is a consistent structural component of the axoneme.

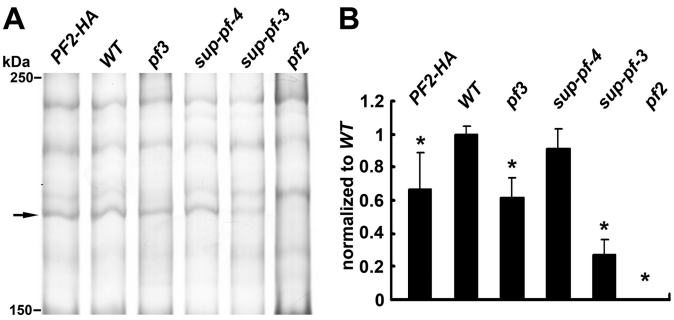

FIGURE 5. **SDS-PAGE analysis of axonemal proteins from WT *Chlamydomonas*, *PF2-HA*, and four *drc* mutants (*pf3*, *sup-pf-4*, *sup-pf-3*, and *pf2*).** *A,* DRC7 is marked with an *arrow* on the 5% SDS-polyacrylamide gel. *B,* relative quantification of DRC7 is based on the average of three independently replicated silver-stained gels and is expressed as the mean ± S.D. *Asterisks* indicate significant changes in comparison with WT ($p < 0.01$).

Two of the polypeptides identified in our MS analysis have previously been shown to be components of other structures within the axoneme and are unlikely to be bona fide subunits of the N-DRC. The first protein, IDA7 (IC140), which was identified in a spot mixed with FAP61, is a well characterized subunit of I1 dynein (45). Our analysis cannot distinguish which of the two polypeptides (or both) caused the changes observed in *drc* mutants. A change in the abundance of IDA7 would be consistent with the observation of connections between I1 dynein and the N-DRC in our recent cryo-ET study (7), suggesting that I1 dynein interacts with the N-DRC. However, null mutants in *IC140* block assembly of I1 dynein with no observed effect on the assembly of the N-DRC (46).

The second protein, FAP119, has been reported to be part of a calmodulin-containing complex located in the C1a projection of the CPC (47), and this protein is completely missing in the *pf6* mutant, which only lacks the C1a projection (47). The observed shifts in the pI of FAP119 in *drc* mutants may indicate that defects in the N-DRC affect the signaling cascade involving calcium modulations to regulate the flagellar waveform. Therefore, we excluded ICL1, IDA7, and FAP119 as *bona fide* subunits of the N-DRC, leaving the seven previously known N-DRC components DRC1–7 and five novel N-DRC or N-DRC-associated candidates, including FAP61, FAP206,

TABLE 2

Identification of previously observed N-DRC candidates in *Chlamydomonas* flagellar axoneme by MALDI-TOF MS

Lines that are clustered with the same shade of gray background highlight groups of spots that were identified as the same protein.

Accession No	Description	Gene	Theor. Mr(Da) /pI	Observ. Mr (kDa)	Mascot score [a]	Sequence coverage (%)	Abundance [b]						Phosphorylation	Spot No.
							WT	*PF2-HA*	*pf3*	*sup-pf-4*	*sup-pf-3*	*pf2*		
? [c]	DRC1	?	?	85.6	?	?	++	++	\	++	++	++	Yes	**4**
				85.2	?	?	+	+	\	+	+	+	Yes	**5**
				84.0	?	?	+++	+++	\	+++	+++	+++	No	**6**
XP_001699103	DRC2	*FAP250*	48510/5.73	70.5	127	48	++++	++++	\	++++	++	+++	No	**15**
				70.9	120	29	+	+	\	+	++	++	Yes	**14**
				71.0	122	33	\	\	\	\	++	+	Yes	**13**
				71.2	153	34	\	\	\	\	++	+	Yes	**12**
XP_001693032	DRC3	*FAP134*	60600/4.75	60.1	182	44	++	++	+	++	+	\	No	**18**
Q7XJ96	DRC4	*PF2*	55074/6.63	55.2	170	47	+++	\	++	+++	\	\	No	**19**
				55.8	181	41	++	\	+	++	\	\	No	**20**
				63.3	134	33	\	+++	\	\	\	\	?	**16**
				62.2	147	38	\	+++	\	\	\	\	?	**17**
				51.50	111	26	\	\	\	\	++	\	No	**21**
				49.1	138	34	\	\	\	\	++	\	No	**22**
XP_001689724	DRC5	*FAP155*	43989/ 6.38	41.0	165	50	+++	+++	+	\	++	\	No	**30**
XP_001703017	DRC6	*FAP169*	28866/8.12	30.6	119	51	++	++	\	\	+	\	No	**44**
XP_001699034	DRC7	*FAP50*	133206/5.53	201.8	175	19	+++	+++	+	+++	+	\	Yes	**1**
				194.2	200	30	+++	+++	+	+++	+	\	Yes	**2**
				199.9	217	28	+++	+++	++	+++	+	\	?	**Band***

[a] Mascot scores are taken from on-line search results from Matrix Science. A mascot score of >70 is considered significant ($p < 0.05$).
[b] Abundance is depicted using +, and increases with the number of +; \ means missing; the comparison is just valid for the same protein.
[c] ? means unknown.
* indicates band from SDS-PAGE.

TABLE 3

Identification of other polypeptides that are altered in *Chlamydomonas drc* mutant axonemes by MALDI-TOF MS

Lines that are clustered with the same shade of gray background highlight groups of spots that were identified as the same protein.

Accession No	Description	Gene	Theor. Mr(Da) /pI	Observ. Mr (kDa)	Mascot score [a]	Sequence coverage (%)	Abundance [b]						Phosphorylation	Spot No.
							WT	*PF2-HA*	*pf3*	*sup-pf-4*	*sup-pf-3*	*pf2*		
Novel DRC candidates with abundance differences														
XP_001703513	flagellar associated protein (CaM-IP-3)	*FAP61/ IDA7*	122048/4.75	141.8	164	34	+++	+++	++	+	+	+	Yes	**3**
AAD45352	inner dynein arm I1 intermediate chain IC140		110204/ 4.86		118	24								
? [c]	?	?	?	72.4	?	?	+++	+++	++	+++	++	+	No	**11**
XP_001695331	isocitrate lyase	*ICL1*	45948/ 5.9	45.8	148	47	+++	+	++	++	+	+	No	**29**
Novel DRC candidates with shift in drc mutants														
XP_001692249	flagellar associated protein	*FAP206*	32852/5.50	82.0	103	46	+++	+++	+	+++	+	+	Yes	**7**
				80.6	105	45	++	++	++	++	++	++	Yes	**8**
				79.5	103	42	++	++	+	+	+	+	Yes	**9**
				77.3	93	43	+++	+++	++++	++++	++++	++++	No	**10**
XP_001689442	flagellar associated protein	*FAP230*	45570/ 6.54	47.8	127	39	++	++	++	++	++	\	Yes	**23**
				47.5	147	53	+	+	+	+	+	\	Yes	**25**
				47.4	102	32	+	+	+	+	+	\	Yes	**26**
				47.3	174	54	+++	+++	+++	+++	+++	\	No	**27**
				48.0	87	22	\	\	\	\	\	++	Yes	**24**
				47.1	128	39	\	\	\	\	\	+++	No	**28**
XP_001698455	flagellar associated protein	*FAP252*	39610/5.69	40.8	100	15	++	++	++	++	++	\	Yes	**31**
				40.0	137	39	+	+	+	+	+	\	Yes	**32**
				39.7	138	27	+	+	+	+	+	\	Yes	**33**
				39.4	82	19	+++	+++	+++	+++	+++	\	No	**38**
				40.0	136	38	++++	++++	++++	++++	++++	\	No	**39**
				39.9	130	29	\	\	\	\	\	++	Yes	**34**
				39.6	98	22	\	\	\	\	\	+	Yes	**35**
				39.2	83	18	\	\	\	\	\	+	Yes	**36**
				38.7	101	40	\	\	\	\	\	+	Yes	**37**
				39.1	75	21	\	\	\	\	\	+++	No	**40**
				38.5	172	48	+	+	+	+	+	++++	No	**41**
XP_001696622	flagellar associated protein	*FAP119*	33786/5.63	37.5	136	53	+	+	+	\	\	\	No	**42**
				36.9	108	42	\	\	\	+	+	+	No	**43**

[a] Mascot scores are taken from the on-line search results from Matrix Science. A mascot score of >70 was considered significant ($p < 0.05$).
[b] The abundance is depicted using +, and increases with the number of +; \ means missing; the comparison is just valid for the same protein.
[c] ? means unknown.

FAP230, FAP252, and spot 11 (Fig. 6). As described above, many of these 12 proteins have different isoforms in WT axonemes. The spot patterns of the N-DRC components show little change in mutants that lack either I1 dynein (*pf9–3*) or radial spokes (*pf14*), with the exception of FAP206, which is reduced in *pf14* (Fig. 6).

Gene Expression Pattern of N-DRC Candidates—Each *drc* mutant is associated with defects in the assembly of multiple axonemal polypeptides; however, with the exception of PF2 (DRC4), the mutant gene products were unknown (13–17). Dikaryon rescue studies have indicated that DRC1 may be the mutant gene product in *pf3* and that DRC5 may be the mutant gene product in *sup-pf-4* (17). To determine whether any of the observed polypeptide defects are caused by changes in the expression of the corresponding N-DRC genes, we performed qRT-PCR for each of the N-DRC components identified here using RNA isolated from both WT and mutant cells. To focus on flagellar proteins, we extracted RNA from WT cells before and 45 min after deflagellation. Transcripts for all tested N-DRC candidates were significantly elevated after deflagellation (Fig. 7*A*), which is consistent with previous studies examining *FAP50*, *FAP169*, *FAP206*, and *FAP230* transcripts (13, 24, 48).

As the expression of axonemal proteins is dynamically regulated throughout the cell cycle (49–52), precise quantification of the transcript abundance of axonemal proteins would require synchronized cells that are harvested at the same cell cycle phase. However, because different mutants grow at different speeds, synchronization is difficult to achieve. Also, different cell lines have flagella of different lengths. For example, the flagella in the *pf3* and *pf2* mutants are only about ¾ of the WT length, whereas the other mutants grow flagella of WT length (16). Therefore, we focused primarily on detecting the defective N-DRC gene in the different *drc* mutants.

The *pf2-4* mutation is a null allele occurring due to the insertion of a large plasmid between exons 4 and 5 of the *PF2* gene (13). Two pairs of *PF2* primers were designed as follows: *PF2-1* amplifies a product spanning exons 3 and 4 (amino acids 77–118), and *PF2-2* amplifies a product spanning exons 5 and 6 (amino acids 194–226). The *PF2-1* product was observed in all strains except for *sup-pf-3*, but the *PF2-2* product was not observed in the *pf2* strain (Fig. 7*B*, *arrowhead*). These results are consistent with the site of the *pf2-4* mutation, earlier observations that the full-length *PF2* transcript is destabilized in this mutant (13), and recent studies on *sup-pf-3*.[6]

[6] D. Tritschler and M. E. Porter, unpublished results.

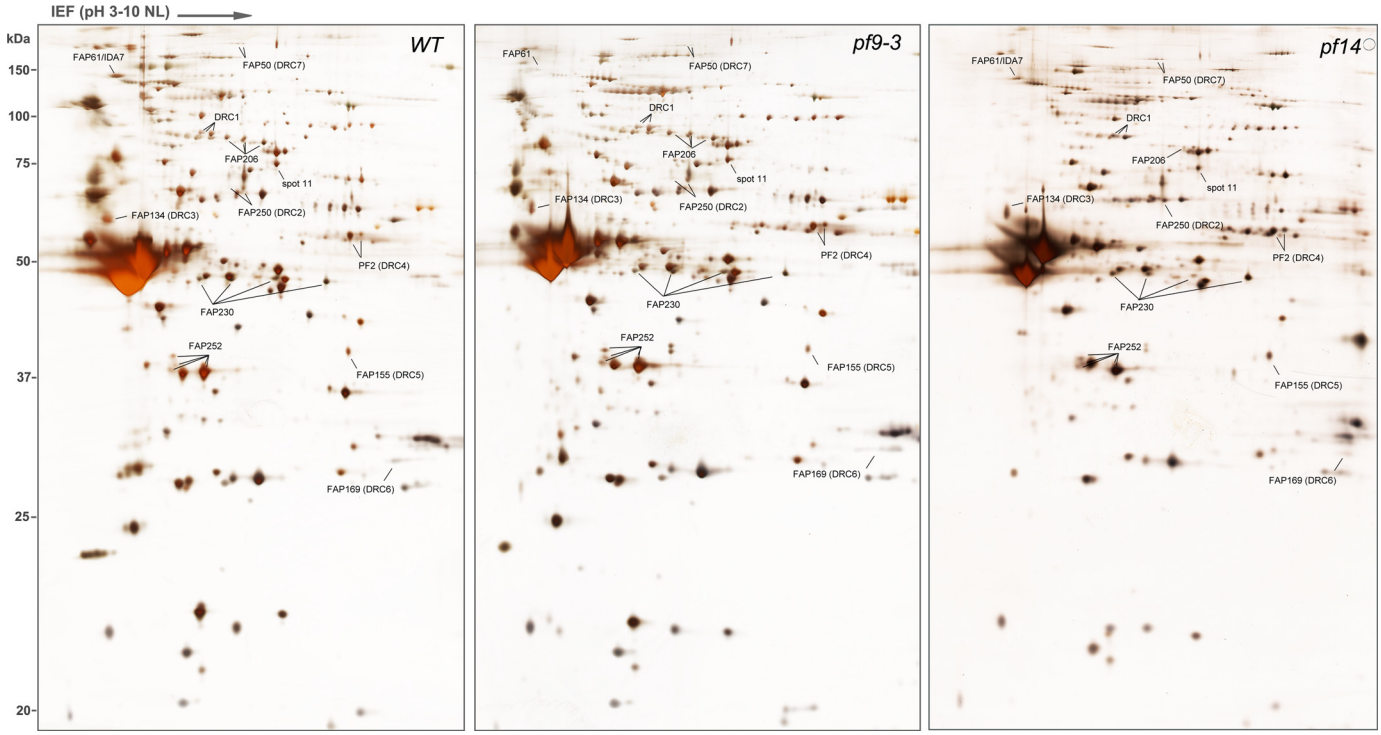

FIGURE 6. **Twelve N-DRC candidates identified by comparative proteomic analysis of WT and *drc* mutants.** No significant changes were observed in the spot patterns of the N-DRC components in mutants that lack either I1 dynein (*pf9-3*) or radial spokes (*pf14*), with the exception of FAP206, which is reduced in *pf14*. Note that many of the N-DRC candidates are present as multiple spots in the silver-stained 2DE gels.

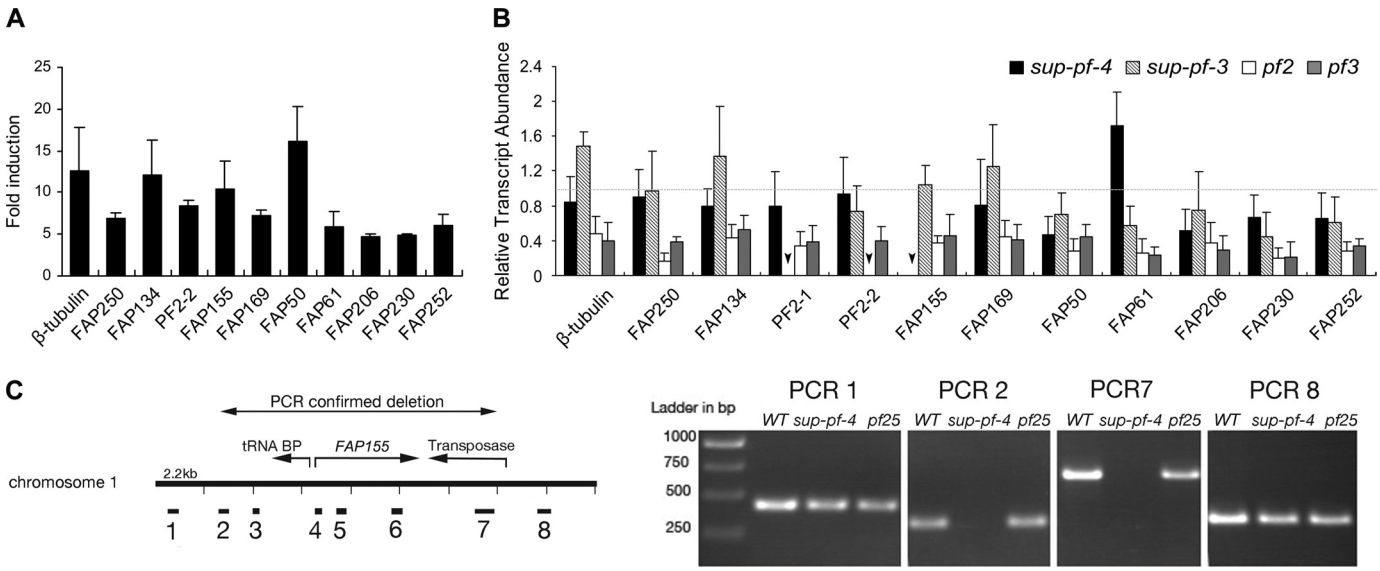

FIGURE 7. **Analysis of N-DRC transcripts in *drc* mutants by qRT-PCR and identification of a gene deletion by genomic PCR.** *A,* changes in the transcript levels of N-DRC candidates after deflagellation were measured by qRT-PCR. *B,* relative abundance of each transcript in the *drc* mutants (*sup-pf-4*, *sup-pf-3*, *pf2*, and *pf3*). *Arrowheads,* qRT-PCR products that were not detected in a given *drc* mutant. *C,* identification of a gene deletion in *sup-pf-4* by genomic PCR. PCR primers were designed for the amplification of genomic DNA fragments in the region around *FAP155*. The positions of PCR products 1–8 are shown in the *left diagram*. The region contains at least three genes, including *FAP155*. The results from agarose gel electrophoresis of genomic PCR products (PCR1, PCR2, PCR7, and PCR8) are shown in the *right panel*.

As mentioned above, dikaryon rescue analysis has previously identified DRC5 as the putative mutant gene product in *sup-pf-4* (17). As *sup-pf-4* only lacks DRC5 (FAP155) and DRC6 (FAP169), we analyzed both genes in *sup-pf-4* by real time PCR, genomic PCR, and DNA sequencing. The *FAP169* transcript was present in *sup-pf-4* at WT level (Fig. 7*B*). PCR amplification and DNA sequencing with overlapping primers spanning the entire *FAP169* gene failed to identify any nucleotide changes in *sup-pf-4* DNA (supplemental Fig. S3 and supplemental Table S1). These results indicate that FAP169 is not the product of the *sup-pf-4* gene. In contrast, qRT-PCR failed to detect a *FAP155* transcript in *sup-pf-4* (Fig. 7*B*, *arrowhead*). We therefore tried to recover the *FAP155* gene from *sup-pf-4* using genomic PCR. Eight pairs of primers spread over a greater than 15-kb region

that includes the *FAP155* gene were used to amplify fragments from WT, *pf25,* and *sup-pf-4* genomic DNA (Fig. 7*C* and supplemental Table S1). The *pf25* mutant is the original host strain used for the isolation of the *sup-pf-4* suppressor and served as the second control strain (15). All eight products were recovered from WT and *pf25* genomic DNA, whereas only the PCR1 and PCR8 products were recovered from *sup-pf-4* DNA (Fig. 7*C*). These results suggest that the *sup-pf-4* mutation was caused by a large deletion (>12.3 kb) of genomic DNA that removed the entire *FAP155* transcription unit and two neighboring genes (Fig. 7*C*).

Homologs and Motifs of the N-DRC Subunits and Candidates—Cilia and flagella are highly conserved organelles. To find potential homologs for the N-DRC components identified here, we used reciprocal BLASTP to explore the genome sequences of several organisms with motile cilia and flagella (*V. carteri*, *S. purpuratus*, *H. sapiens*, and *T. brucei*), only nonmotile cilia (*C. elegans*), and without cilia and flagella (*A. thaliana*). Previous work has shown that both DRC4 (PF2) and FAP61 (CaM-IP3) are highly conserved in organisms with motile cilia (13, 48). Using an *e* value of $1e^{-15}$ as the cutoff for homology, homologs of DRC2, -3, and -5 were found in organisms with motile axonemes but not in organisms with only nonmotile cilia (*C. elegans*) or no cilia (*A. thaliana*) (Table 4). For FAP50 (DRC7), the largest protein associated with the N-DRC, we found three categories of sequence similarities (Table 4) as follows: (*a*) high similarity throughout the entire sequence of FAP50 with a reciprocal best match of the closely related, multicellular green alga *V. carteri*; (*b*) sequence similarity of the C-terminal half of FAP50 with a reciprocal best match only in organisms that have motile cilia and flagella; these similarities are strong in a highly conserved region around amino acids 580–800 (Table 4) that has no predicted motifs or defined domains, followed by one to three segments with moderate similarities; and (*c*) sequence similarities of regions in the N-terminal half of FAP50 with various proteins in all explored organisms; however, these homology scores are mainly based on leucine-rich repeat (LRR) domains or Kelch motifs, and with one exception (NP_001189691.1 of *A. thaliana*), none of these proteins are reciprocal best matches with FAP50. Homologs of DRC6, FAP206, FAP230, and FAP252 were not identified in other organism except for *V. carteri*.

We used bioinformatics programs to predict domains and structural motifs (Table 4) in the N-DRC gene products of *Chlamydomonas*. Coiled-coil regions were the most commonly identified domains, which is not surprising as these domains are often found in large protein complexes and can mediate protein-protein interactions. LRR domains were the second most common; these domains are also known to be involved in protein-protein interactions. DRC7 was particularly rich in protein-protein interaction domains, with coiled-coil, LRR, and Kelch domains. As described previously (48), FAP61 (CaM-IP3) does not contain any of the abovementioned interaction domains, but it does contain an acyl-CoA *N*-acyltransferase domain and a pyridine nucleotide-disulfide oxidoreductase (Pyr-redox) domain. These domains function in metabolic activities and suggest a potential role in energy recycling in the axoneme. FAP252 has two EF-hand domains, known to be involved in Ca^{2+}

TABLE 4
Predicted homologs, domain, and motif architectures of N-DRC candidates

Protein	NCBI-BlastP result[a]							Predicted domains/motifs
	Organisms with motile cilia or flagella				Organisms without motile cilia			
	V. carteri (taxid:3067)	*S. purpuratus* (taxid:7668)	*H. sapiens* (taxid:9606)	*T. brucei* (taxid:5691)	*A. thaliana* (taxid:3702)	*C. elegans* (taxid:6239)		
FAP250 (DRC2)	XP_002953818.1 (1–330; $4e^{-178}$)	XP_790738.1 (1–395; $2e^{-94}$)	NP_149115.2 (1–395; $8e^{-76}$)	XP_828802.1 (1–395; $1e^{-53}$)	\[b]	\		Coiled-coil region
FAP134 (DRC3)	XP_002947561.1 (1–509; 0)	XP_797673.1 (4–506; $3e^{-76}$)	NP_001123562.1 (11–506; $6e^{-66}$)	XP_845620.1 (7–507; $8e^{-37}$)	\	\		Coiled-coil region; LRR_1 (IPR001611)
PF2[c] (DRC4)	XP_002954934.1 (1–471; 0)	XP_782050.2 (15–468; $2e^{-145}$)	NP_001472.1 (24–468; $1e^{-140}$)	XP_827655.1 (44–446; $8e^{-86}$)	\	\		Coiled-coil region
FAP155 (DRC5)	XP_002953885.1 (1–390; $6e^{-171}$)	XP_797414.1 (10–380; $4e^{-48}$)	NP_872345.2 (6–380; $1e^{-39}$)	XP_844901.1(7–377; $4e^{-25}$)	\	\		LRR_1 (IPR001611)
FAP169 (DRC6)	XP_002948058.1 (1–260; $5e^{-104}$)	\	\	\	\	\		\
FAP50 (DRC7)[d]	XP_002945646.1 (1–761; 0)	XP_795345.2 (584–749; $1e^{-30}$)	EAW82947.1 (590–818; $8e^{-35}$)	XP_844724.1 (583–757; $1e^{-29}$)	NP_001189691.1 (334–520; $2e^{-22}$)	NP_741391.2 (53–225; $1e^{-21}$)		Coiled-coil region; LRR_1 (IPR001611); Kelch_1 (IPR006652); Kelch_2 (IPR011498)
FAP61[c] (CaM-IP3)	XP_002955935.1 (370–1121; 0)	XP_783801.2 (395–1127; $9e^{-68}$)	NP_056400.2 (395–1120; $5e^{-57}$)	XP_845755.1 (572–948; $6e^{-17}$)	\	\		Acyl-CoA *N*-acyltransferase (IPR016181); Pyr_redox_2 (Pfam)
FAP206	XP_002951973.1 (106–257; $2e^{-19}$)	\	\	\	\	\		\
FAP230	XP_002947130.1 (1–447; $7e^{-105}$)	\	\	\	\	\		EPSP_SYNTHASE_1(IPR001986)
FAP252	XP_002949979.1 (4–352; 0)	\	\	\	\	\		EF hand (IPR002048/Pfam)

[a] Data in parentheses under predicted homolog indicate the aligned region (amino acid number) and expected value; only aligned regions with an *e* value of less than $1e^{-15}$ are listed.
[b] "\" indicates none identified.
[c] Homology information and predicted motifs in PF2 (DRC4) and FAP61 (CaM-IP3) were previously reported in Refs. 13 and 48.
[d] All proteins except for NP_741391.2 are mutual best fit to FAP50.

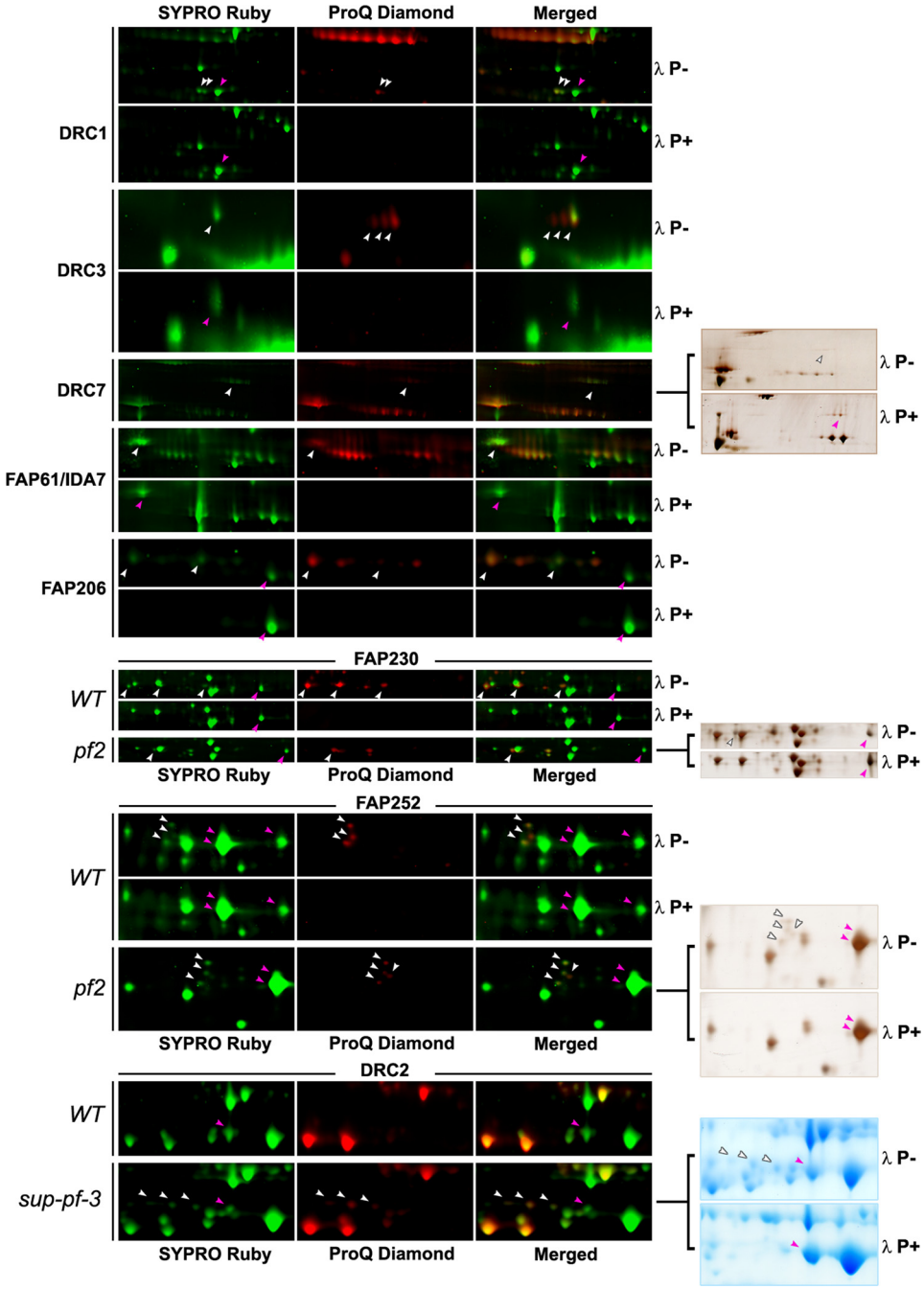

FIGURE 8. **Close-up images of 2DE gel spots stained for comparative phosphorylation analysis.** Unless otherwise indicated, images are from WT axonemes. For most proteins, six images are displayed; the *upper* and *lower rows* show the spot pattern in the absence (λ *P*−) or presence (λ *P*+) of λ-phosphatase, respectively. Phosphorylated isoforms (*white arrowheads*) were detected by comparison of phosphoprotein stain (ProQ Diamond, *red spots*) and total protein stain (SYPRO Ruby, *green spots*; silver stain, *brown spots*; or Coomassie stain, *blue spots*). Nonphosphorylated isoforms (*magenta arrowheads*) were only detected by total protein staining. For proteins FAP230, FAP252, and DRC2, a WT-to-mutant comparison is shown (see the label on the *left* of the last three image blocks).

binding. FAP230 has an EPSP synthase domain, which is essential (and unique) to plants, fungi, and bacteria.

Phosphoproteome of the N-DRC Complex—Phosphorylation is known to play an essential role in the signaling mechanism in cilia and flagella, and thus, it may also be critical for the regulatory function of the N-DRC. A detailed characterization of N-DRC phosphorylation may lead to a better understanding of regulatory switches in this complex. To characterize the phosphorylation status of the N-DRC and N-DRC-associated proteins identified here, we used two related approaches as follows: (*a*) phosphoprotein-specific staining (ProQ Diamond dye) of 2DE gels and (*b*) λ-phosphatase treatment of the axonemal proteins. λ-Phosphatase treatment dephosphorylates phosphoserine, phosphothreonine, phosphotyrosine, and phosphohistidine residues (35, 36), causing a shift of the affected proteins toward a more basic position on 2DE gels.

SYPRO Ruby (for total protein staining) successfully detected all the N-DRC candidate spots, whereas ProQ Diamond specifically detected a phosphorylated subset for most of the N-DRC candidates: DRC1–3 and -7, FAP61/IDA7 (spot 3),

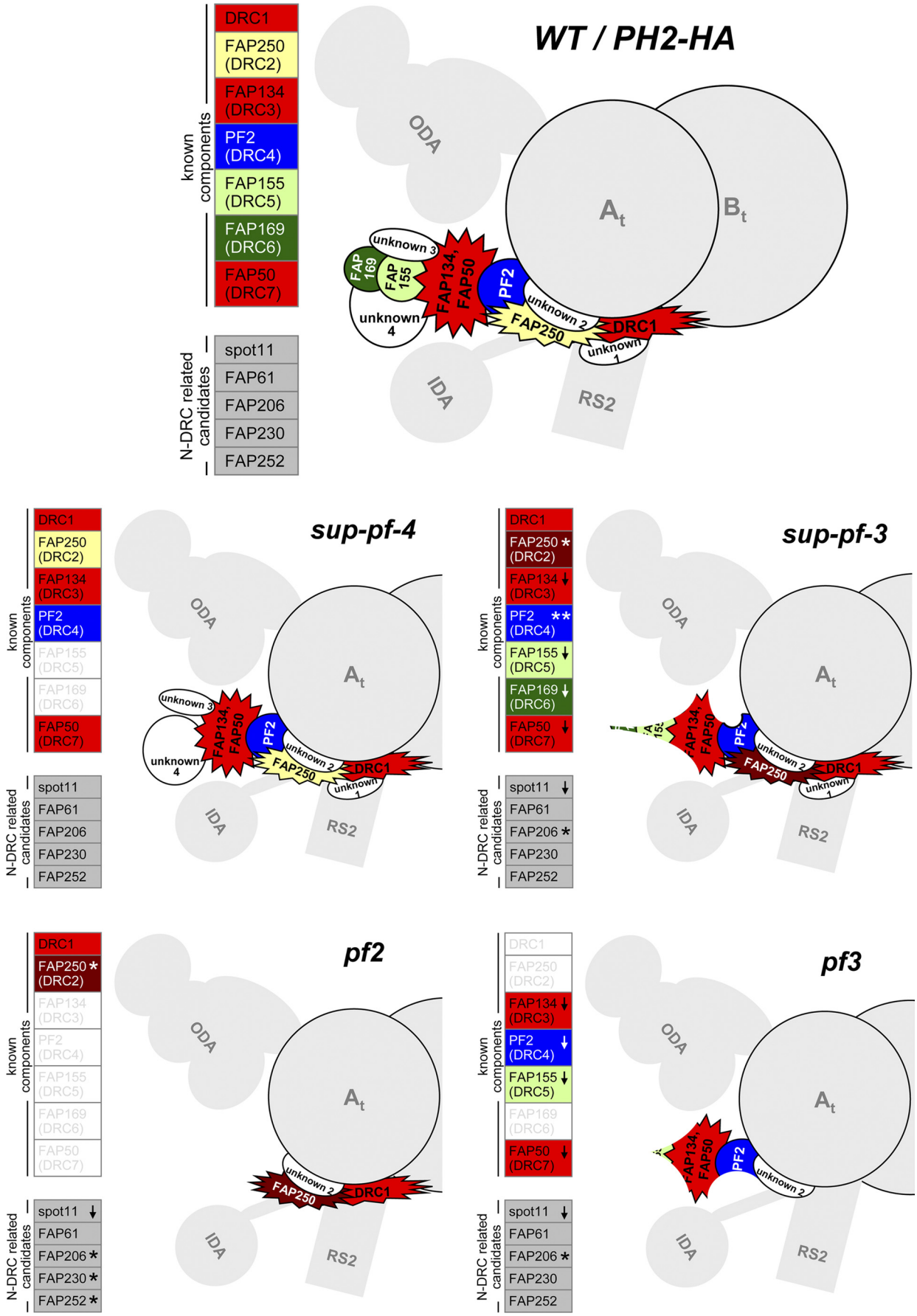
WT / PH2-HA
known components
DRC1
FAP250 (DRC2)
FAP134 (DRC3)
PF2 (DRC4)
FAP155 (DRC5)
FAP169 (DRC6)
FAP50 (DRC7)
N-DRC related candidates
spot11
FAP61
FAP206
FAP230
FAP252
ODA
A_t
B_t
IDA
RS2
unknown 3
FAP 169
FAP 155
FAP134, FAP50
PF2
unknown 4
unknown 2
FAP250
DRC1
unknown 1
sup-pf-4
sup-pf-3
pf2
pf3

FAP206, FAP230, and FAP252 (Fig. 8 and supplemental Fig. S4). Each of these proteins exhibited several phosphorylated isoforms. All of the spots identified by ProQ Diamond (excluding tubulin) disappeared or were reduced after λ-phosphatase treatment (Fig. 8, *white arrowheads*, and supplemental Fig. S4), and a corresponding increase was seen in the spots that represent the nonphosphorylated isoforms, detected only by total protein staining (Fig. 8, *magenta arrowheads*). These observations suggest that these proteins contain multiple phosphorylation sites and exist in several differentially phosphorylated states.

As described above, DRC2 (FAP250) and FAP206 showed significant differences in the abundance of individual spots in some *drc* mutants but no significant change in the total amount of protein (Figs. 3 and 4). The results of the phosphoproteomic analysis indicate that these changes are due to shifts in the phosphorylation state of the proteins (Fig. 8). Intriguingly, three phosphorylated DRC2 isoforms exist in *pf2* and *sup-pf-3*, whereas only one phosphorylated isoform is weakly detected in WT *Chlamydomonas* and the other *drc* mutants (Fig. 3). These results indicate a significant increase in DRC2 phosphorylation in *pf2* and *sup-pf-3*. FAP206 shows a different pattern, in that all four isoforms are present in all strains. However, the relative intensity of the phosphorylated spots (spots 7 and 8) decreases and is shifted toward dephosphorylated states in the *pf3*, *pf2,* and *sup-pf3* mutants (Fig. 4).

DRC1, -3, and -7 generated a series of phosphorylated spots in WT and various *drc* mutants. Although their total protein levels may be altered in different mutants, the extent of phosphorylation remained relatively constant in the different mutants tested (Figs. 3 and 8). Even though we detected several phosphorylated isoforms for FAP230 and FAP252, the locations of those spots do not overlap with the locations of the shifted spots for these proteins in *pf2* axonemes. In fact, for both proteins, the relative amount of phosphorylated isoforms appears to be unchanged between WT and *pf2*. Instead, the spot patterns are shifted as a whole in the first dimension (pI) in *pf2* (Figs. 4 and 8).

DISCUSSION

Conservation and Evolution of the N-DRC Proteome—Homology searches show that 6 of 10 N-DRC candidates (FAP250, FAP155, FAP134, FAP61, FAP50, and PF2) have potential homologs in species with motile cilia (Table 4). This result supports the hypothesis that the N-DRC is a highly conserved part of the regulatory system that coordinates the activity of axonemal dynein. This homology is also consistent with a previous study indicating that these proteins are conserved in motile cilia and flagella (53).

In our study, FAP250 (DRC2) showed the highest variation in phosphorylation between WT and the *drc* mutants. Both the human homolog, the testis development protein NYD-SP28, and the ascidian sea squirt (*Ciona intestinalis*) homolog, SMC83, are sperm tail proteins that undergo phosphorylation in response to sperm activation (54, 55). This homology suggests that the phosphorylation status of FAP250 is important for the regulatory function of the N-DRC.

Two of the N-DRC proteins map to genetic loci linked to human diseases with a known or suspected ciliary basis (3, 53). The human homolog of FAP134 (DRC3), "leucine-rich repeat containing 48 isoform A," is linked to retinal cone dystrophy (53), and the homolog of FAP155 (DRC5), TCTE 1, which has been found in the sperm of all mammalian species examined to date, maps to a locus linked to spinocerebellar ataxia and epilepsy (56).

PF2 (DRC4) is the most thoroughly studied N-DRC component to date, and previous studies have demonstrated that mutations of the *DRC4* gene (*PF2*) cause defects in *C. reinhardtii* N-DRC assembly (13) and that mutations in the DRC4 homologs trypanin and GAS8 disrupt the cilia-dependent step of the *Trypanosoma* life cycle (4) as well as cause defects typical of ciliary diseases in zebrafish (31), respectively. A human homolog, GAS11, binds microtubules (57) but has not yet been directly linked to ciliary motility. However, the growing evidence clearly points to an important and conserved role for this protein in ciliary function.

FAP61 is a new N-DRC candidate, and genomic comparisons suggest that there are homologs in species with motile cilia. Unfortunately, none of the homologs has been studied thoroughly as yet. Interestingly, however, in *C. reinhardtii,* this protein (also named CaM-IP3) seems to be a member of the conserved CaM- and radial spoke-associated complex (CSC), which plays a role in calcium modulation of the flagellar waveform through the CPC·RS signaling pathway (48). Although this study did not explore the relationship between the N-DRC and CSC, previous immunoprecipitation experiments have indicated that the association of CSC with CaM is disrupted in *pf2* and *pf3* mutants, whereas CSC components can still be coimmunoprecipitated with one another in these two *drc* mutants (48). In this study, further interpretation of the data is complicated because the FAP61 spot is mixed with IDA7 (IC140). However, the basic shift of FAP252 in *pf2*, FAP119 (a member of a CaM-containing complex) in *sup-pf-4*, *sup-pf-3*, and *pf2*, and the possible reduction of FAP61 (a member of the CSC) in *drc* mutants suggest that the N-DRC is involved in the transduction of Ca^{2+} signals to mediate regulatory signals between the CPC·RS and dynein arms.

FAP50 (DRC7) shows different levels of sequence similarity with potential homologs in other species. First, the high similarity and close relationship of the organisms clearly indicates that FAP50 is the *Chlamydomonas* ortholog of

FIGURE 9. **Models for the N-DRC in *Chlamydomonas* WT and *drc* mutants.** The probable locations of the N-DRC components are based on this study and previous structural results (7). Legends on the *left* of each diagram indicate the N-DRC candidates in each strain. The following labels and color codes for subunits were used: reduced proteins are indicated with *downward arrows*, and missing proteins are faded out on a *white background*; proteins with PTM changes are labeled with an *asterisk*, and truncated PF2 is labeled with *two asterisks*. The PTM annotations are based on our phosphoproteomic analysis of the N-DRC. *Star-shaped* blocks indicate N-DRC candidates with phosphorylated isoforms. The *changing colors* of FAP250 in *sup-pf-3* and *pf2* indicate the changes in phosphorylation status in these *drc* mutants. The interactions among candidate N-DRC proteins require further confirmation, and little is known about the stoichiometry of the candidates. A_t, A-tubule; B_t, B-tubule; *RS2*, radial spoke 2; *IDA*, inner dynein arm; *ODA*, outer dynein arm. For a detailed explanation, see the text.

XP_002945646.1 in *V. carteri*. Second, the high sequence similarities of the region around amino acids 580–800 of FAP50 with reciprocal best matches, which is followed by segments with moderate similarities to the same proteins, suggest that the entire C-terminal half of FAP50 is conserved in organisms with motile cilia and flagella. This C-terminal region, which has no predicted motifs or defined domains, can be matched to the human protein EAW82947.1 (GENE ID: 84229 CCDC135). This interpretation is consistent with previous studies that reported FAP50 as the reciprocal best match to this vertebrate protein, as well as localized it to doublet microtubules, and showed that it is involved in the regulation of flagellar motility (24, 58). The third type of predicted homology is weaker and applies to small regions in the N-terminal half of FAP50 that are predicted to form Kelch and LRR domains. These motif-based N-terminal sequence similarities were found for organisms both with and without motile cilia, and although they indicate putative domain homology, they are unlikely to represent orthology. For example, the human BAF84937.1 (a testis protein) shows similarity to the N-terminal half of FAP50 with a relatively low BLASTP *e* value of $2e^{-20}$ because of an extended LRR domain; however, these proteins are not the reciprocal best matches. It is also possible that domains within the N-terminal half of FAP50 have yet to be identified and possibly universal function(s), which could explain the sequence similarities with proteins in nonciliated organisms. For example, it has previously been shown that intraflagellar transport polypeptides, which are essential for ciliary assembly, are also found in lymphoid and myeloid cells that lack primary cilia, where they are required for formation of the immune synapse (59).

Defects in drc Mutants—N-DRC candidates were identified based on changes in the axonemal protein level, which could be caused either directly by a mutation of the respective gene or by an assembly defect, preventing the localization of the protein to the axoneme. Previous dikaryon rescue experiments tentatively identified DRC1, -4, and -5 as the putative mutant gene products in *pf3*, *pf2,* and *sup-pf-4*, respectively (17). DRC4 was later identified as the *PF2* gene product by rescue of the *pf2-4* mutant phenotype with both WT and epitope-tagged DRC4 constructs (13). Here, we have extended this work by integrating proteomic, qRT-PCR, and genomic PCR data, corroborating the previously indicated gene products.

Both *pf2* and *sup-pf-3* have defects in the assembly of DRC4 (Tables 1 and 2). In *pf2-4* cells, the *DRC4* gene is truncated by plasmid insertion between exons 4 and 5 (13). We were able to detect an RT-PCR product in *pf2* for exons 3 and 4 but not for exons 5 and 6 (Fig. 7*B*), consistent with earlier studies (13). No truncated DRC4 protein product has been detected in *pf2*, but even if it exists, it fails to provide the scaffold necessary for the assembly of several other N-DRC components into the axoneme, as shown by both two- and three-dimensional electron microscopy (7, 13). We also observed that DRC4 is truncated in *sup-pf-3*, consistent with previous work.[7]

Our results reveal that the *FAP155* gene is located within an ~12-kb region of genomic DNA that is deleted in *sup-pf-4*. These results suggest that the deletion of *FAP155* could be responsible for the *sup-pf-4* phenotype, although final confirmation will require rescue of *sup-pf-4* by transformation with the WT gene. Our MS/PMF analysis failed to identify a sequence associated with the DRC1 spots, but we could detect transcripts for the other two N-DRC subunits missing in the *pf3* mutant, FAP250 (DRC2) and FAP169 (DRC6). One of several possible explanations is that DRC1 is the mutant gene product in *pf3*, which would be consistent with previous dikaryon rescue results (17).

N-DRC Assembly—Previously, DRC1–7 were found to be localized within the N-DRC using cryo-ET to compare the three-dimensional structures present in WT *Chlamydomonas* and missing in the *drc* mutants. Specifically, DRC1 and -2 are located in the base plate; DRC3, -4, and -7 are found in the linker domain, and DRC5 and -6 are localized to the distal lobe of the linker of the N-DRC (Fig. 1) (7). This study provides a more complete model for the subunit composition of the N-DRC and identifies the specific defects of the *drc* mutants (Fig. 9).

PF2 (DRC4) seems to serve as a scaffold that facilitates the assembly of FAP134 (DRC3), FAP155 (DRC5), FAP169 (DRC6), and FAP50 (DRC7) into the N-DRC, which is consistent with previous studies (7, 13). FAP134 and FAP50 are still assembled in *sup-pf-3* but at significantly reduced levels, which, in correlation with our cryo-ET data (7), indicate that these subunits may connect to the inner dyneins. Both DRC1 and FAP250 (DRC2) are missing in *pf3* and seem to be components of the base plate that facilitates the attachment of the N-DRC to the A-tubule. The loss of one or both of these polypeptides may also be responsible for the decrease of PF2 (DRC4) in *pf3*. Both FAP155 and FAP169 are part of the distal linker, and the *pf3*, *sup-pf3,* and *sup-pf-4* data suggest that FAP155 is necessary for the assembly of FAP169.

In our previous cryo-ET study, we indicated four structural blocks ("unknown 1–4") that could not be correlated with the known N-DRC components (Fig. 1) (7). "Unknown 1" (a base plate protrusion) appears to only interact with the base plate and is missing in *pf3* and *pf2*. "Unknown 3 and 4" are part of the linker and are missing in *sup-pf-3*, *pf3*, and *pf2*. Although our results and the previous cryo-ET study (7) suggest that the components in unknown 3 and 4 assemble into the N-DRC in a FAP134- and FAP50-dependent manner, we could not unambiguously identify the proteins present in the unknown densities 1, 3, and 4. This inability could be due to multiple factors as follows: (*a*) Some of what appears to be "missing" in the three-dimensional structure comparison actually exists in the mutant but is absent in the sub-tomogram averages due to increased flexibility of subunits in the N-DRC as a result of missing anchor points and/or connections. (*b*) One known limitation of 2DE gels is the inability to resolve high molecular weight proteins (above 200 kDa in size). (*c*) To ensure reliability of the proteomic data, a stringent cutoff was chosen to identify statistically significant changes in protein levels, and it is therefore possible that we missed some smaller, but potentially real, changes using this method. For example, reduced levels of tektin have previously been observed for *pf3* axonemes by SDS-PAGE and Western blot (14, 16, 17, 30). Although we detected altered tektin levels in our 2DE analysis, these changes were not

[7] R. Bower, J. Mueller, D. Tritschler, C. Perrone, I. Dorweiler, and M. E. Porter, unpublished data.

statistically significant, possibly due to the complicated distribution pattern of tektin in our 2DE gels (supplemental Fig. S1) (phosphorylated isoforms manifested as a string of spots). "Unknown 2" is located in what is likely to be a critical region in the center of the N-DRC and showed no difference in EM density in any of the *drc* mutants (7). It is possible that the novel N-DRC candidates FAP206, FAP230, and/or FAP252 localize to this density, as they showed WT abundance in the *drc* mutants, yet exhibited unique changes in PTM. If so, they may serve as docking proteins for DRC4 and other DRC4-dependent N-DRC components. Alternatively, these proteins may not directly be a part of the N-DRC but rather components of one of the many connections to neighboring axonemal structures (7). The observed reduction in FAP206 levels in the radial spoke null mutant *pf14* supports the possibility that it serves as a signal transducer between radial spokes and the N-DRC.

Two recent studies have identified *CCDC39* and *CCDC40*, which are genes linked to PCD, as potential N-DRC components in human cilia (60, 61). The protein products of both genes localize to ciliary axonemes and are essential for assembly of inner dynein arms and the N-DRC (60, 61). The *Chlamydomonas* homologs of CCDC39 and CCDC40 are FAP59 and FAP172, respectively. The migration of FAP59 suggests phosphorylated isoforms (supplemental Fig. S1), and the pattern is the same in the *drc* mutants. FAP172 has not been identified in our 2DE gels. The lack of changes in the *drc* mutants suggests that both proteins may localize to the unknown 2 intensity, serving as N-DRC docking proteins, or to other N-DRC-associated structures, similarly to FAP206, FAP230, and FAP252. The proteomic patterns of FAP61 (mixed spot) and spot 11 did not match directly to the cryo-ET density pattern, and the localization of these subunits will require further study.

Phosphorylation Is a Key PTM in the N-DRC—Reversible protein phosphorylation is one of the main regulatory mechanisms in the cell, and (de)phosphorylation of the I1-intermediate chain IC138 has already been shown to play a critical role in dynein regulation in response to CPC·RS signaling (11, 12, 18, 62–64). Eight of the proteins identified here (FAP50 (DRC7), FAP61, FAP134 (DRC3), FAP206, FAP230, FAP250 (DRC2), FAP252, and DRC1) are post-translationally modified by phosphorylation, and the isoform patterns are affected by the genotype, suggesting that reversible phosphorylation is also a key regulatory mechanism for the N-DRC.

Using immobilized metal affinity chromatography to enrich for phosphopeptides, a previous phosphoproteomic study found 32 phosphoproteins in *Chlamydomonas* flagella (26). However, FAP230 was the only N-DRC candidate detected as a phosphoprotein in this study. This discrepancy may be due to the different techniques used for identifying phosphoproteins. Affinity purification is likely less sensitive than the phosphoprotein dye and phosphatase treatment experiments used here. Alternatively, the PTM may have been preserved less effectively in the previous study due to additional fractionation steps. The quality of structure preservation in this study was confirmed by ATP reactivation of the purified axonemes (data not shown).

Interestingly, changes in the phosphorylation levels of FAP250 (DRC2) and FAP206 in certain *drc* mutants seemed to be inversely correlated, and both were rescued in the *PF2-HA* strain (Figs. 3 and 4). FAP206 phosphorylation was reduced when FAP250 was either hyper-phosphorylated in *sup-pf-3* and *pf2* or missing in *pf3*. Proper phosphorylation of FAP250 homologs has previously been shown to be important for the activity of sperm flagella (54, 55). Together, these data suggest that FAP250, like IC138, serves as a phosphorylation target during regulatory signaling. Given that hyper-phosphorylation of FAP250 occurs in *pf2* and *sup-pf3*, and proper phosphorylation is restored in *PF2-HA*, it appears that PF2 (DRC4) or some of the proteins recruited by it are directly involved in the regulation of FAP250 phosphorylation. Initiation of such signaling may also involve CaM complexes, as has been shown for the regulation of I1 dynein (48).

In conclusion, we have identified the protein and gene sequences of the previously named N-DRC components, DRC2–7, and identified five novel N-DRC candidates or N-DRC-associated proteins with significant changes in *drc* mutants. Our data suggest that phosphorylation of N-DRC components is a key PTM in this regulatory complex and that FAP250 and/or FAP206 is/are involved in the regulatory mechanism through (de)phosphorylation. Combining this information with previous studies, we were able to assemble new models of the N-DRC in WT and *drc* mutants, leading to future studies focusing on the activities of individual N-DRC components.

Acknowledgments—We thank Noreen R. Francis for technical assistance; Raqual Bower (University of Minnesota) for providing the PF2 rescued strain; the Brandeis University Mass Spectrometry (BUMS) Facility directed by Dr. Jeff Agar for access to their instruments; Michael Rosbash for use of instruments; Douglas Theobald for advice on Bioinformatic analysis; and J. Richard McIntosh for critical reading of the manuscript.

REFERENCES

1. Fliegauf, M., Benzing, T., and Omran, H. (2007) *Nat. Rev. Mol. Cell Biol.* **8,** 880–893
2. Marshall, W. F., and Kintner, C. (2008) *Curr. Opin. Cell Biol.* **20,** 48–52
3. Broadhead, R., Dawe, H. R., Farr, H., Griffiths, S., Hart, S. R., Portman, N., Shaw, M. K., Ginger, M. L., Gaskell, S. J., McKean, P. G., and Gull, K. (2006) *Nature* **440,** 224–227
4. Ralston, K. S., and Hill, K. L. (2006) *PLoS Pathog.* **2,** e101
5. Porter, M. E., and Sale, W. S. (2000) *J. Cell Biol.* **151,** F37–F42
6. Nicastro, D., Schwartz, C., Pierson, J., Gaudette, R., Porter, M. E., and McIntosh, J. R. (2006) *Science* **313,** 944–948
7. Heuser, T., Raytchev, M., Krell, J., Porter, M. E., and Nicastro, D. (2009) *J. Cell Biol.* **187,** 921–933
8. Satir, P. (1968) *J. Cell Biol.* **39,** 77–94
9. Summers, K. E., and Gibbons, I. R. (1971) *Proc. Natl. Acad. Sci. U.S.A.* **68,** 3092–3096
10. Smith, E. F., and Yang, P. (2004) *Cell Motil. Cytoskeleton* **57,** 8–17
11. Wirschell, M., Hendrickson, T., and Sale, W. S. (2007) *Cell Motil. Cytoskeleton* **64,** 569–579
12. Wirschell, M., Yang, C., Yang, P., Fox, L., Yanagisawa, H. A., Kamiya, R., Witman, G. B., Porter, M. E., and Sale, W. S. (2009) *Mol. Biol. Cell* **20,** 3044–3054
13. Rupp, G., and Porter, M. E. (2003) *J. Cell Biol.* **162,** 47–57
14. Gardner, L. C., O'Toole, E., Perrone, C. A., Giddings, T., and Porter, M. E. (1994) *J. Cell Biol.* **127,** 1311–1325
15. Huang, B., Ramanis, Z., and Luck, D. J. (1982) *Cell* **28,** 115–124
16. Piperno, G., Mead, K., and Shestak, W. (1992) *J. Cell Biol.* **118,** 1455–1463
17. Piperno, G., Mead, K., LeDizet, M., and Moscatelli, A. (1994) *J. Cell Biol.* **125,** 1109–1117

18. Habermacher, G., and Sale, W. S. (1997) *J. Cell Biol.* **136,** 167–176
19. King, S. J., and Dutcher, S. K. (1997) *J. Cell Biol.* **136,** 177–191
20. San Agustin, J. T., and Witman, G. B. (1994) *Cell Motil. Cytoskeleton* **27,** 206–218
21. Yang, P., and Sale, W. S. (2000) *J. Biol. Chem.* **275,** 18905–18912
22. Gaillard, A. R., Diener, D. R., Rosenbaum, J. L., and Sale, W. S. (2001) *J. Cell Biol.* **153,** 443–448
23. Smith, E. F. (2002) *Cell Motil. Cytoskeleton* **52,** 33–42
24. Pazour, G. J., Agrin, N., Leszyk, J., and Witman, G. B. (2005) *J. Cell Biol.* **170,** 103–113
25. Piperno, G., Huang, B., Ramanis, Z., and Luck, D. J. (1981) *J. Cell Biol.* **88,** 73–79
26. Boesger, J., Wagner, V., Weisheit, W., and Mittag, M. (2009) *Eukaryot. Cell* **8,** 922–932
27. Brokaw, C. J., and Luck, D. J. (1985) *Cell Motil.* **5,** 195–208
28. Brokaw, C. J., and Kamiya, R. (1987) *Cell Motil. Cytoskeleton* **8,** 68–75
29. Mastronarde, D. N., O'Toole, E. T., McDonald, K. L., McIntosh, J. R., and Porter, M. E. (1992) *J. Cell Biol.* **118,** 1145–1162
30. Yanagisawa, H. A., and Kamiya, R. (2004) *Mol. Biol. Cell* **15,** 2105–2115
31. Colantonio, J. R., Vermot, J., Wu, D., Langenbacher, A. D., Fraser, S., Chen, J. N., and Hill, K. L. (2009) *Nature* **457,** 205–209
32. Gorman, D. S., and Levine, R. P. (1965) *Proc. Natl. Acad. Sci. U.S.A.* **54,** 1665–1669
33. Witman, G. B., Carlson, K., Berliner, J., and Rosenbaum, J. L. (1972) *J. Cell Biol.* **54,** 507–539
34. Rupp, G., O'Toole, E., Gardner, L. C., Mitchell, B. F., and Porter, M. E. (1996) *J. Cell Biol.* **135,** 1853–1865
35. Yamagata, A., Kristensen, D. B., Takeda, Y., Miyamoto, Y., Okada, K., Inamatsu, M., and Yoshizato, K. (2002) *Proteomics* **2,** 1267–1276
36. Raggiaschi, R., Lorenzetto, C., Diodato, E., Caricasole, A., Gotta, S., and Terstappen, G. C. (2006) *Proteomics* **6,** 748–756
37. Lin, J. F., Xu, J., Tian, H. Y., Gao, X., Chen, Q. X., Gu, Q., Xu, G. J., Song, J. D., and Zhao, F. K. (2007) *Int. J. Cancer* **121,** 2596–2605
38. Livak, K. J., and Schmittgen, T. D. (2001) *Methods* **25,** 402–408
39. Moseley, J. L., Chang, C. W., and Grossman, A. R. (2006) *Eukaryot. Cell* **5,** 26–44
40. Nematollahi, G., Kianianmomeni, A., and Hallmann, A. (2006) *BMC Genomics* **7,** 321
41. Schloss, J. A. (1990) *Mol. Gen. Genet.* **221,** 443–452
42. Altschul, S. F., Madden, T. L., Schäffer, A. A., Zhang, J., Zhang, Z., Miller, W., and Lipman, D. J. (1997) *Nucleic Acids Res.* **25,** 3389–3402
43. Kabututu, Z. P., Thayer, M., Melehani, J. H., and Hill, K. L. (2010) *J. Cell Sci.* **123,** 3587–3595
44. Chamberlain, K. L., Miller, S. H., and Keller, L. R. (2008) *Genetics* **179,** 7–19
45. Yang, P., and Sale, W. S. (1998) *Mol. Biol. Cell* **9,** 3335–3349
46. Perrone, C. A., Yang, P., O'Toole, E., Sale, W. S., and Porter, M. E. (1998) *Mol. Biol. Cell* **9,** 3351–3365
47. Wargo, M. J., Dymek, E. E., and Smith, E. F. (2005) *J. Cell Sci.* **118,** 4655–4665
48. Dymek, E. E., and Smith, E. F. (2007) *J. Cell Biol.* **179,** 515–526
49. Weeks, D. P., and Collis, P. S. (1979) *Dev. Biol.* **69,** 400–407
50. Tuxhorn, J., Daise, T., and Dentler, W. L. (1998) *Cell Motil. Cytoskeleton* **40,** 133–146
51. Pan, J., and Snell, W. J. (2005) *Dev. Cell* **9,** 431–438
52. Wilson, N. F., Iyer, J. K., Buchheim, J. A., and Meek, W. (2008) *Semin. Cell Dev. Biol.* **19,** 494–501
53. Baron, D. M., Ralston, K. S., Kabututu, Z. P., and Hill, K. L. (2007) *J. Cell Sci.* **120,** 478–491
54. Zheng, Y., Zhang, J., Wang, L., Zhou, Z., Xu, M., Li, J., and Sha, J. H. (2006) *Int. J. Mol. Med.* **18,** 1119–1125
55. Hozumi, A., Padma, P., Toda, T., Ide, H., and Inaba, K. (2008) *Cell Motil. Cytoskeleton* **65,** 249–267
56. Juneja, R., Agulnik, S. I., and Silver, L. M. (1998) *J. Androl.* **19,** 183–188
57. Becker-Heck, A., Zohn, I. E., Okabe, N., Pollock, A., Lenhart, K. B., Sullivan-Brown, J., McSheene, J., Loges, N. T., Olbrich, H., Haeffner, K., Fliegauf, M., Horvath, J., Reinhardt, R., Nielsen, K. G., Marthin, J. K., Baktai, G., Anderson, K. V., Geisler, R., Niswander, L., Omran, H., and Burdine, R. D. (2011) *Nat. Genet.* **43,** 79–84
58. Yang, Y., Cochran, D. A., Gargano, M. D., King, I., Samhat, N. K., Burger, B. P., Sabourin, K. R., Hou, Y., Awata, J., Parry, D. A., Marshall, W. F., Witman, G. B., and Lu, X. (2011) *Mol. Biol. Cell* **7,** 976–987
59. Finetti, F., Paccani, S. R., Riparbelli, M. G., Giacomello, E., Perinetti, G., Pazour, G. J., Rosenbaum, J. L., and Baldari, C. T. (2009) *Nat. Cell Biol.* **11,** 1332–1339
60. Bekker, J. M., Colantonio, J. R., Stephens, A. D., Clarke, W. T., King, S. J., Hill, K. L., and Crosbie, R. H. (2007) *Cell Motil. Cytoskeleton* **64,** 461–473
61. 61 Merveille, A. C., Davis, E. E., Becker-Heck, A., Legendre, M., Amirav, I., Bataille, G., Belmont, J., Beydon, N., Billen, F., Clément, A., Clercx, C., Coste, A., Crosbie, R., de Blic, J., Deleuze, S., Duquesnoy, P., Escalier, D., Escudier, E., Fliegauf, M., Horvath, J., Hill, K., Jorissen, M., Just, J., Kispert, A., Lathrop, M., Loges, N. T., Marthin, J. K., Momozawa, Y., Montantin, G., Nielsen, K. G., Olbrich, H., Papon, J. F., Rayet, I., Roger, G., Schmidts, M., Tenreiro, H., Towbin, J. A., Zelenika, D., Zentgraf, H., Georges, M., Lequarré, A. S., Katsanis, N., Omran, H., and Amselem, S. (2011) *Nat. Genet.* **43,** 72–78
62. Bower, R., VanderWaal, K., O'Toole, E., Fox, L., Perrone, C., Mueller, J., Wirschell, M., Kamiya, R., Sale, W. S., and Porter, M. E. (2009) *Mol. Biol. Cell* **20,** 3055–3063
63. Habermacher, G., and Sale, W. S. (1996) *J. Cell Sci.* **109,** 1899–1907
64. Hendrickson, T. W., Perrone, C. A., Griffin, P., Wuichet, K., Mueller, J., Yang, P., Porter, M. E., and Sale, W. S. (2004) *Mol. Biol. Cell* **15,** 5431–5442
65. Myster, S. H., Knott, J. A., O'Toole, E., and Porter, M. E. (1997) *Mol. Biol. Cell* **8,** 607–620